Evaluating the performance of honeycomb briquettes produced from semi-coke and corn stover char

Evaluating the performance of honeycomb briquettes produced from semi-coke and corn stover char: Co-combustion, emission characteristics, and a value-chain model for rural China

Hongbin Cong[a], Lixin Zhao[a,*], Ondřej Mašek[b], Zonglu Yao[a], Haibo Meng[a], Lili Huo[a], Yanwen Yuan[a], Jixiu Jia[a], Yunong Wu[a]

[a]Center of Energy and Environmental Protection, Chinese Academy of Agricultural Engineering Planning & Design, Beijing 100125, China

[b]University of Edinburgh, School of Geosciences, UK Biochar Research Centre, King's Buildings, Edinburgh EH93FF, UK

***Corresponding author:** Tel./fax: +86 010 59196810.

E-mail address: zhaolixin5092@163.com

ABSTRACT: A honeycomb briquette made from semi-coke and corn stover char was developed as a possible heating fuel in rural China. In this study, the co-combustion characteristics of semi-coke and corn stover char combined in different proportions were tested and analyzed. It was determined that adding 20 % corn stover char (BS28) effectively improved the combustion performance of semi-coke, and this proportion was regarded as the ideal mixing ratio. Thus, the integrated combustion characteristics of the blend improved to 15.08×10^{-12} $K^{-3}\cdot min^{-2}$ compared to 5.44×10^{-12} $K^{-3}\cdot min^{-2}$ for semi-coke alone. The emission test results revealed that SO_2 and $PM_{2.5}$ emissions decreased with corn stover char addition; however, NO_X emissions increased and the combustion efficiency decreased slightly with corn stover char addition. The SO_2 concentrations resulting from the combustion of BriqCK, Briq28, and Briq46 (honeycomb briquettes with ratios of char to semi-coke of 0:10, 2:8, and 4:6, respectively) under different experimental conditions were 24.9–26.3, 9.5–16.7, and 5.2–15.4 mg/Nm^3, respectively, and the NO_X concentrations were 63.1–149.7, 54.3–175.4, and 57.7–168.4 mg/Nm^3, respectively. A value-chain model for the new heating fuel was developed and possible benefits were analyzed. If either the new investment cost or raw material input costs ($25 USD/t of straw char) were subsidized by national public finance, then the project would be profitable and run sustainably. This study provided an important technical basis for the development and application of new heating fuels in China.

Keywords: co-combustion; air pollution emission; corn stover char; semi-coke; honeycomb briquette[1]

1. Introduction

The amount of collectible crop straw (e.g., from corn, wheat, rice, and cotton) in China was approximately 900 million tons during recent five years (MOA, 2016). A large amount of crop straw has been burned directly in open fields. This open field burning has serious implications for air pollution, traffic accidents, and overall fire risk. Instead of open field burning, if these crop residues were properly utilized as fuel, then China's reliance on coal as a primary energy source would be expected to decrease (Chen, 2016; Sun, 2016). Straw char produced by slow pyrolysis consists mainly of carbon, minerals, and metals (EBC, 2018; Klinghoffer et al., 2011). There are numerous beneficial possibilities for its use, including waste management, climate change mitigation, and clean energy production (Gómez et al., 2016; Kua et al., 2019; Li et al., 2019). Owing to properties that make it a clean and renewable fuel, it is feasible to explore efficient methods, such as densification, to upgrade straw char into high value-added bioenergy (Hu et al., 2015). The widespread use of straw char requires the development of adequate utilization strategies to achieve economic and environmental sustainability of bioenergy chains (Barbanera et al., 2018).

The Chinese government's 13th Five-Year Plan for Energy Development proposes to replace conventional coal with clean energy sources, including natural

[1]Originally a honeycomb-shaped block molded using only coal, which is the main household fuel for many residents in East Asia.

63 gas, electric power, clean coal, and renewable energy, for heating in northern China
64 (NEA, 2017). Semi-coke is an industrial product of bituminous raw coal produced by
65 low-temperature carbonization (Jie et al., 2018). It is considered a potential
66 replacement for raw coal (MEP, 2016) because it has a high fixed carbon content,
67 high calorific value, and low ash, sulfur, and phosphorus contents. Replacing
68 traditional raw coal with semi-coke briquettes could effectively improve
69 environmental outcomes (Li et al., 2016; Li et al., 2016a), as the use of semi-coke
70 briquettes has the potential to reduce emissions compared with those from current
71 coal consumption in China (Jie et al., 2018).
72 Straw char's high alkali and alkaline earth metals (AAEMs) content may cause
73 several operating problems in the combustion system (Hernández et al., 2016);
74 however, they can weaken the polymer chain and catalyze the combustion of semi-
75 coke (Peng et al., 2015). Compared with semi-coke, straw char has higher
76 hydrophobicity but lower densification performance (Hu, 2015). Despite the large
77 number of studies on the co-combustion characteristics of biomass with char, sludge,
78 and oil shale (Liu et al., 2015; Niu et al., 2017; Sarkar et al., 2014), there remains a
79 considerable knowledge gap in the development of a new fuel blended from straw
80 char and semi-coke, which are produced by similar processes using different raw
81 feedstocks. Information pertaining to the emissions from the combustion of
82 honeycomb briquettes produced from a combination of semi-coke and straw char is
83 also very limited (Li et al., 2016a; Yank, 2016), which affects the development and

84 promotion of new heating fuels.

85 The primary objective of this study was to investigate the influence of variations
86 in corn stover char blending proportions on the combustion characteristics of semi-
87 coke, and to determine the emission characteristics of a new honeycomb briquette
88 molded from a combination of corn stover char and semi-coke. In addition, a value-
89 chain model for honeycomb briquette production and utilization was designed, and
90 the expected benefits based on the model were analyzed. This provided essential data
91 for the development and application of a new heating briquette produced from a
92 combination of straw char and semi-coke.

93 **2. Materials and methods**

94 ***2.1 Characterization of materials***

95 The test materials primarily included corn stover char, semi-coke, and
96 honeycomb briquettes molded from different blends of these two fuels. Corn stover
97 char was produced using a pilot-scale rotary kiln at a pyrolysis temperature of 600 °C
98 and a residence time of 30 min (Cong et al., 2017). Semi-coke was obtained directly
99 from the market; it was produced by low-temperature carbonization of highly volatile
100 bituminous coal from Shenmu County, Shaanxi Province, which is the largest semi-
101 coke production base in China. Blends of corn stover char and semi-coke for the
102 combustion characteristics test were marked with BC×× (Table 1). Based on the
103 results of the co-combustion characteristics analysis, the ratios of corn stover char to
104 semi-coke of 2:8 and 4:6 (BS28 and BS46) were selected for analysis in the pollution

emission study, and the blends were molded into honeycomb briquettes with a pressure of 21kN; meanwhile, honeycomb briquettes molded from semi-coke alone were also used for comparative analysis. The honeycomb briquettes were marked with Briq×× (Table 1). Finally, 6 % kaolin and 1.5 % glutinous rice flour (by mass) were added to the main ingredients to improve the densification performance when the honeycomb briquettes were molded.

Table 1. Summary of abbreviations used for the various mixtures and honeycomb briquettes

Abbreviations	BS28	BS46	BS64	BS82	BriqCK	Briq28	Briq46
Corn straw char: semi-coke (by mass)	2:8	4:6	6:4	8:2	0:10	2:8	4:6

Before compression molding, the raw materials were milled through a 4 mm mesh. Table 2 presents the characteristics of the raw materials. Heating values were measured using a bomb calorimeter (LECO AC-300) following the adiabatic method according to the China national standard (GB T 213-2008). The ultimate analysis (carbon, hydrogen, nitrogen, and sulfur) was determined using a Vario ELIII Elemental Analyzer according to ASTM 5373 and ASTM 4239. The metal element contents were determined by inductively coupled plasma mass spectrometry (Thermo Fisher Scientific) according to AOAC Official Method 975. 03.

Table 2. Characteristics of the raw materials

Material		Corn stover char	Semi-coke
Particle size [mm]		⩽4	⩽4
Bulk density[a] [kg/m^3]		264.79	750.28
LHV[b] [MJ/kg]		22.53	23.32
Proximate analysis [wt % ad]	Moisture	2.78	10.28
	Volatile	10.08	13.97
	Ash	31.81	19.89
	Fixed carbon	55.33	55.86
Ultimate analysis [wt % daf]	C	65.86	70.04
	H	2.19	0.46
	O[c]	30.45	28.60
	N	1.46	0.62
	S	0.04	0.28
Metal elements [mg/g]	Na	1.35	0.23
	K	35.23	0.12
	Ca	23.02	0.48
	Mg	11.46	0.02
	Al	2.32	0.02
	Si	0.11	0.01

ad: air-dry basis; daf: dry and ash-free basis

[a]Tested according to the methods of the dust character test (the China national

126 standard GB/T16913-2008)

127 [b]LHV: lower heating value

128 [c]Calculated by the difference

129 ***2.2 Experimental facility***

130 An NF9C household heating stove (Laowan Biomass Technology Co., Ltd.,

131 China) was used in this study; raw coal briquettes are frequently used to power this

132 type of stove in rural areas of northern China. The stove had a hearth height of 650

133 mm, an outer length × width of 480×480 mm, and an inner diameter of 230 mm (Fig.

134 1). It had an enclosed combustion chamber, circulating water system, and an air inlet

135 with a diameter of 60 mm near the stove bottom. The air inlet was set up with open

136 ratios of 0 %, 40 %, 70 %, and 100 % during various experiments to examine

137 emissions. Special honeycomb briquettes with a height of 100 mm, an outer diameter

138 of 220 mm, and 19 holes with a diameter of 26 mm were used in this study.

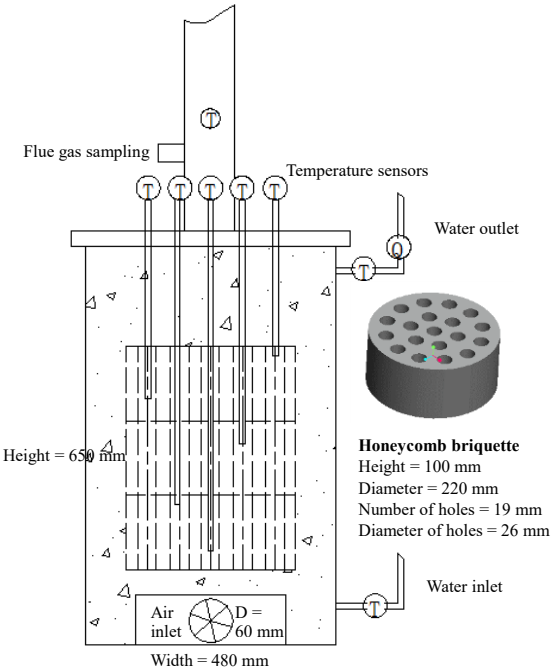

Fig. 1. Testing system based on a household heating stove from rural China using the special honeycomb briquettes.

2.3 Analytical methods

In this study, a thermogravimetric analyzer (STA409PC) manufactured by NETZSCH was used to analyze the combustion characteristics, and the test results were smoothed using Proteus 5.3 software. The reactor had a diameter of 60 mm, and the reaction atmosphere was canned air. The surface of the crucible (6 mm inner diameter) was uniformly coated with 5–10 mg samples and then covered with a platinum cap provided by NETZSCH. The initial temperature of the test was set at 30 °C; it was raised to 930 °C at a heating rate of 10 °C/min. The air flow rate was 100 mL/min. These settings were similar to those used in previous related studies

(Niu et al., 2017; Sarkar et al., 2014).

Total suspended particles (TSP) were collected using an electrical low-pressure impactor (Dekati ELPI+) manufactured by DEKATI Ltd., which can collect particles from 6 nm to about 10 μm in 14 size fractions. The mass size distributions and the number size distributions of the TSP were estimated using ELPI software V12.0. To ensure that the collected particulate matter was kept below saturation, the flue gas was diluted 64 times using two Dekati diluters.

A flue gas analyzer (ECOM-J2KN) manufactured by RBR was used to test the NO_X, SO_2, CO, and CO_2 emissions, and the flue gas was sampled three times, once every 4 minutes. The results were converted from ppm to mg/Nm^3.

Combustion characteristics were evaluated using several combustion parameters (e.g., ignition temperature, burnout temperature, burnout characteristics, and integrated combustion characteristics), as previously described (Moon et al., 2013). The burnout index (C_b) (10^{-4}/min) was used to characterize the burnout characteristics of the sample; large values indicated a greater burnout performance.

$$C_b = \frac{f_1 \cdot f_2}{t_0}, \quad (1)$$

where f_1 (%) is the initial burnout rate, which characterizes the loss rate of fuel weight on the ignition point of the thermogravimetry (TG) curve (a large value represents greater flammability of the fuel); f_2 (%) is the late burnout rate; and t_0 (min) is the burnout time, which represents the time from the initiation of combustion mass loss to burnout (with a mass loss rate of 98 %).

The integrated combustion characteristics of the sample were described by the combustion index (S_N) (10^{-12} $K^{-3}\cdot min^{-2}$); larger values indicated a greater burning performance of the sample.

$$S_N = \frac{(dw/dt)_{max}\cdot(dw/dt)_{mean}}{t_i^2 t_f}, \quad (2)$$

where $(dw/dt)_{max}$ (%/min) is the maximum burn rate, $(dw/dt)_{mean}$ (%/min) is the average burn rate, t_i (K) is the ignition temperature, and t_b (K) is the burnout temperature.

The China national standard GB 18484-2001 was used to calculate the CE (combustion efficiency; %) based on the concentrations of CO and CO_2.

$$CE = \frac{C_{CO2}}{C_{CO2}+C_{CO}} \times 100\ \%, \quad (3)$$

where C_{CO2} and C_{CO} are the test concentrations of CO_2 and CO in the flue gas (%), respectively.

3. Results and discussion

3.1 Co-combustion characteristics

3.1.1 Combustion characteristic curves of corn stover char and semi-coke

The thermogravimetry (TG), differential thermogravimetry (DTG), and differential scanning calorimetry (DSC) curves of the semi-coke and corn stover char were tested. As shown in Fig. 2, the weight loss and exothermic processes of the two fuels were clearly different. When the samples were heated, water evaporated, which was accompanied by devolatilization, volatile flaming, and fixed carbon firing (Zhao et al., 2014). Before the heating temperature reached 100 °C, the semi-coke

194 experienced a high reduction in weight owing to the loss of its relatively high
195 moisture content (Table 1). Corn stover char exhibited a more intense rate of weight
196 loss during the second stage; this occurred at a relatively lower temperature than that
197 for semi-coke.

198 The char exhibited a faster rate of weight loss and a narrower exothermic
199 duration. The combustion performance of corn stover char was better than that of
200 semi-coke. The burnout characteristic index and the integrated combustion index of
201 the char were 100.17×10^{-4}/min and 35.73×10^{-12} $K^{-3}\cdot min^{-2}$, respectively, while the two
202 indexes of the semi-coke were 48.28×10^{-4}/min and 5.44×10^{-12} $K^{-3}\cdot min^{-2}$, respectively.
203

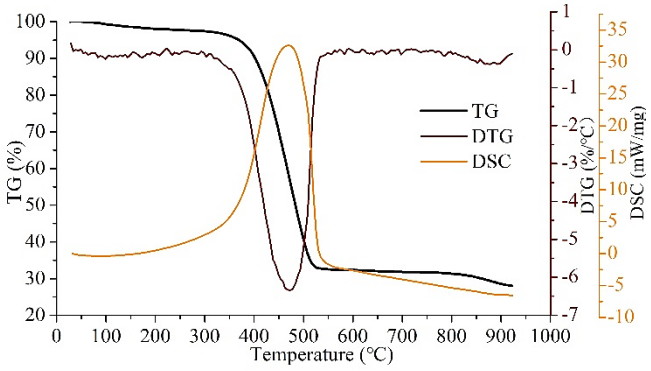

204

205 (a)

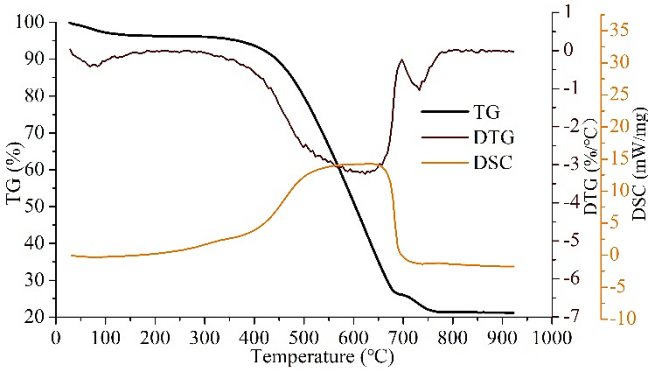

206

(b)

Fig. 2. Combustion characteristic curves (The thermogravimetry (TG), differential thermogravimetry (DTG), and differential scanning calorimetry (DSC) curves) of corn stover char (a) and semi-coke (b).

3.1.2 Co-combustion curves and their interaction

The theoretical thermogravimetry (TG_{cal}) curves, theoretical differential thermogravimetry (DTG_{cal}) curves, and theoretical differential scanning calorimetry (DSC_{cal}) curves were calculated using the proportional superposition method based on the ratio of corn stover char to semi-coke and test results presented in Fig. 2 (Xing et al., 2019), and were compared with the test-derived curves (TG_{exp}, DTG_{exp}, and DSC_{exp}). These are all shown in Fig. 3.

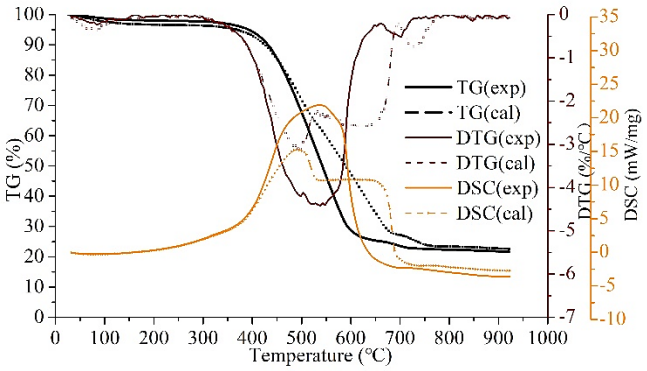

(a)

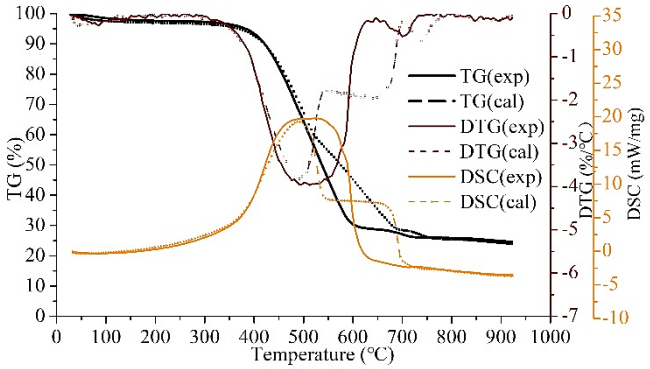

(b)

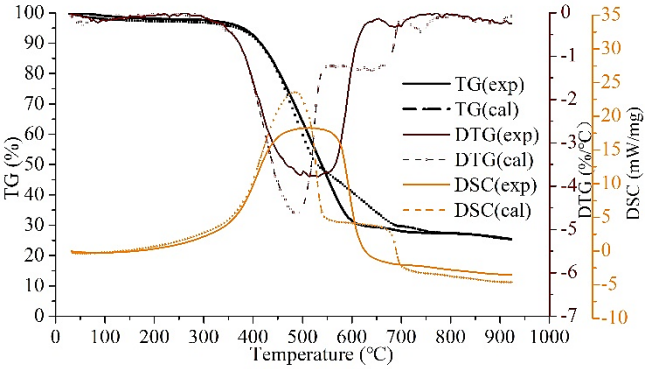

(c)

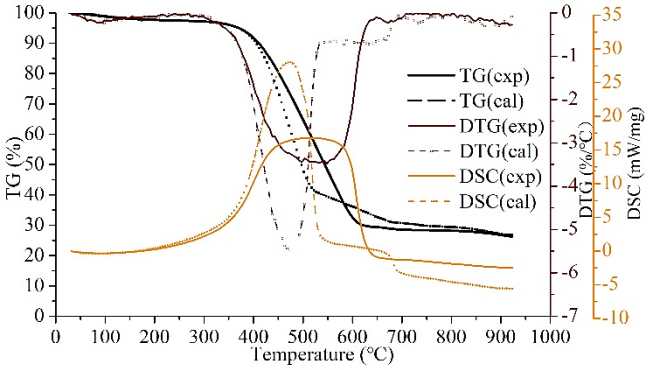

(d)

Fig. 3. Theoretical (subscripted with cal) and test-derived (subscripted with exp) co-combustion characteristic curves (thermogravimetry (TG), differential thermogravimetry (DTG), and differential scanning calorimetry (DSC) curves) of

229 blends BS28 (a), BS46 (b), BS64 (c), and BS82 (d).

230 All test-derived TG curves were smoother than the theoretical TG curves, thereby
231 indicating that there was an interaction between the two fuels during their co-firing.
232 Furthermore, the test-derived TG_{exp} curve of BS28 shifted distinctly to the left of the
233 TG_{cal} curve, and this phenomenon was also reflected in the DSC and DTG curves.
234 The peaks of the DSC_{exp} and DTG_{exp} curves were distinctly larger than those of the
235 DSC_{cal} and DTG_{cal} curves for BS28. As the proportion of corn stover char increased,
236 the extent of the left shift of the curve decreased. Consequently, the TG_{exp} curves of
237 BS46 and BS64 were similar to the TG_{cal} curves. By contrast, the TG_{exp} curve of
238 BS82 showed a distinct shift to the right, and this phenomenon was also reflected in
239 the DSC and DTG curves. The peaks of the DSC_{exp} and DTG_{exp} curves were smaller
240 than those of the DSC_{cal} and DTG_{cal} curves for BS82, respectively.

241 According to the above analysis, it was apparent that when the proportion of char
242 was less than 40 % of the total, the combustion performance of the semi-coke
243 improved. However, a small amount of semi-coke added to char (20 % in the test)
244 resulted in a strong inhibition of char combustion. This might have been due to the
245 fact that some AAEMs (e.g., potassium, sodium, calcium, and magnesium) in the
246 straw char weakened the polymer chain and catalyzed the combustion of semi-coke
247 (Mourant et al., 2011; Peng et al., 2015), while a small amount of semi-coke hindered
248 the diffusion of the flame during char combustion, thereby exhibiting a distinct flame
249 retardant effect (Sarkar et al., 2014).

3.1.3 Co-combustion characteristic indexes

Table 3 shows the combustion characteristic indexes of different samples. The ignition temperature decreased from 429.1 °C (BS28) to 404.9 °C (BS82) as the proportion of char increased, which was consistent with the theoretical trend. However, the burnout characteristic indexes decreased as the proportion of char increased, and ranged from 54.78×10^{-4}/min for BS28 to 48.49×10^{-4}/min for BS82. The maximum and average reaction rates also showed similar trends. In addition, the integrated combustion indexes of BS28, BS46, BS64, and BS82 were 15.08, 13.53, 12.27, and 10.31×10^{-12} $K^{-3}\cdot min^{-2}$, respectively, which indicated a contradictory tendency when compared with the theoretical values. The quantitative study also demonstrated that a small amount of char addition (≤40 %) was more effective at improving the combustion characteristics of semi-coke than the addition of a large amount of char (≥60 %), even though the combustion characteristics of corn stover char were distinctly better than those of semi-coke.

Table 3. Combustion indexes of the samples

Sample	Ignition temperature (℃)	Burnout temperature (℃)	Burnout characteristics (C_b) (10^{-4}/min)	Maximum reaction rate $(dw/dt)_{max}$ (%/min)	Average reaction rate $(dw/dt)_{mean}$ (%/min)	Integrated combustion characteristics (SN) (10^{-12} $K^{-3}\cdot min^{-2}$)
Semi-coke	459.1	693.1	48.28	-3.27	-2.43	5.44
BS28	429.1	601.4	54.78	-4.42	-3.78	15.08
BS46	414.0	593.8	50.00	-3.97	-3.47	13.53
BS64	410.8	595.5	52.76	-3.79	-3.25	12.27
BS82	404.9	603.1	48.49	-3.48	-2.93	10.31
Biochar	401.6	518.1	100.17	-6.35	-4.70	35.73

3.2 Air pollution emissions of honeycomb briquettes

3.2.1 Conventional gaseous pollutant emissions

NO_X and SO_2 emissions are generally regarded as the main conventional gaseous pollutants. As the opening ratio of the air inlet increased, the NO_X concentrations of all briquettes increased (Fig. 4a). The NO_X concentrations of BriqCK, Briq28, and Briq46 were 63.1–149.7, 54.3–175.4, and 57.7–168.4 mg/Nm^3, respectively, as the opening ratio increased from 0 % to 100 %. This trend could be explained as follows. First, at temperatures below 1300 °C, only fuel-NO_X was expected (De Soete, 1990; Werther, 2000) and the correlation between fuel nitrogen and NO_X emissions was significant (Roy, 2012). The nitrogen content in corn stover char was more than double that found in semi-coke. With the increasing proportion of corn stover char, the fuel nitrogen content of the honeycomb briquettes increased, thereby causing increased NO_X concentrations (Jin et al., 2016). The NO_X emissions from biomass may be lower or higher than those from coal owing to the fact that the nitrogen content of different biomasses varies widely (Ren et al., 2017). Second, the stove temperature increased with the increasing opening ratio of the air inlet, and the higher flame temperature resulted in more NO_X being generated (Courtemanche and Levendis, 1998). However, the NO_X concentrations for the new fuels were always lower than the limiting value of 200 mg/Nm^3 of the China national standard (GB 2014-4365) under all experimental conditions.

The SO_2 concentrations of BriqCK, Briq28, and Briq46 under different

experimental conditions were 24.9–26.3, 9.5–16.7, and 5.2–15.4 mg/Nm^3, respectively (Fig. 4b). Overall, the SO_2 emissions were highest from BriqCK and lowest from Briq46. With the increasing proportion of corn stover char, the SO_2 concentration decreased. The sulfur content in the char was approximately 15 % of that in the semi-coke. The SO_2 emissions varied as a function of fuel-bound sulfur, and the AAEMs in corn stover char were potent absorbers of SO_2 (Tarelho et al., 2005; Werther, 2000; Zhang et al., 2019). The SO_2 emissions of Briq28 and Briq46 exhibited a weak downward trend as the opening ratio of the air inlet increased; the higher flame temperature enhanced the SO_2 capture ability of the AAEMs (Zhang et al., 2019). For BriqCK, as the opening ratio of the air inlet increased, the SO_2 concentration tended to slightly increase. The relatively higher flame temperature caused by the larger air inlet opening ratio resulted in a higher conversion rate of fuel sulfur to gaseous SO_2, as has been previously observed (Zhang et al., 2016; Zheng et al., 2013).

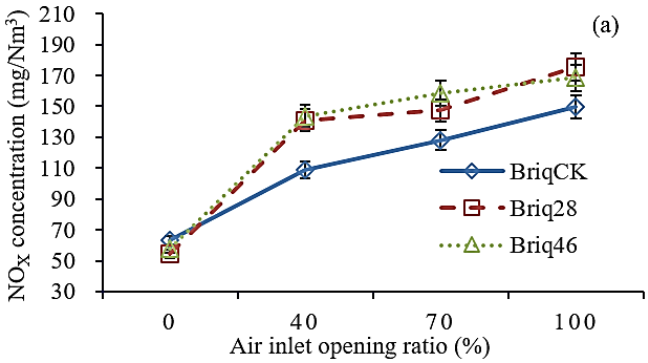

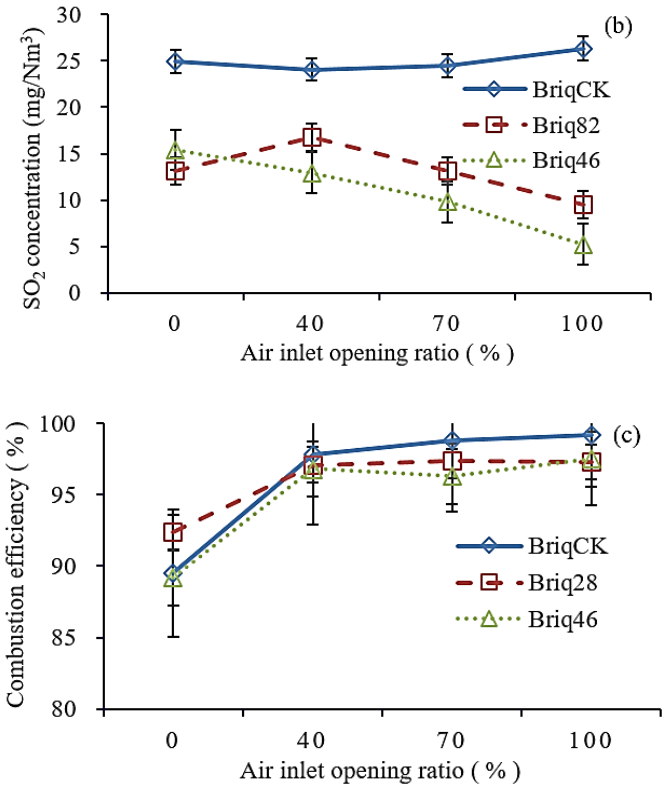

Fig. 4. Concentrations of NO_X (a) and SO_2 (b) and the combustion efficiencies (c) for different honeycomb briquettes.

The concentrations of CO and CO_2 were also used to evaluate the CE according to Equation (3). The CEs of BriqCK, Briq28, and Briq46 are shown in Fig. 4c, respectively. There was a decrease in the CE with the addition of corn stover char. However, the CEs under all experimental conditions, except for the opening ratio of the air inlet of 0 %, exceeded 97.1 %. Although corn stover char addition did not seriously deteriorate the CE in this stove, it may be better to use a specific stove with a secondary airflow for the new fuels, as has been suggested previously (Phusrimuang

et al., 2015; Toscano et al., 2014).

3.2.2 Total suspended particles emissions

Emissions of total suspended particles (TSP), as well as their mass size concentrations and number size concentrations versus different honeycomb briquettes and different operating conditions (the air inlet open ratios of 0 %, 40 %, 70 %, and 100 %, respectively), are shown in Fig. 5. The TSP concentrations were 13.45–18.96 mg/Nm^3 for BriqCK, and these increased linearly with the increasing opening ratio of the air inlet. This might have been related to the rate of burning of the honeycomb briquettes and airflow speed, as it has been previously revealed that the $PM_{2.5}$ concentration increases under intense flaming conditions for clean-burning stoves (Wang et al., 2016). The TSP concentrations of Briq28 and Briq46 were 8.82–11.80 mg/Nm^3 and 8.71–11.63 mg/Nm^3, respectively. As a whole, with the addition of char, the TSP concentrations decreased; this might have been caused by the lower TSP emissions of the char compared with those of the semi-coke and the presence of aluminosilicates in the semi-coke, which were responsible for capturing gaseous species from the char (Wang et al., 2019).

All briquette samples generally presented a similar distribution of mass and number concentrations at various particle sizes as a function of experimental conditions, and all the peaks of the number size concentrations occurred at <0.156 μm. PM_{10} (<10 μm) mainly consisted of $PM_{2.5}$ (<2.5 μm) for all samples, thereby representing more than 99 % of the total number of particles. A similar distribution

was also previously observed by another researcher using wood pellets (Schmidt et al., 2018). The peak values of Briq28 and Briq46 were smaller than that for BriqCK. Taking the operation conditions with an air inlet opening ratio of 100 % as an example, the particle numbers of Briq28 at <0.156 μm and <2.47 μm decreased by 72.4 % and 73.1 %, respectively, compared with those of BriqCK, while those of Briq46 decreased by 80.0 % and 80.3 %, respectively. The addition of corn stover char reduced the emissions of fine particles ($PM_{2.5}$), which are known to adversely affect human health. The mass size concentration data revealed that most particles were larger than 1.63 μm; when the air inlet opening ratio was 100 %, these particles accounted for 95.89 %, 96.51 %, and 96.30 % of the total mass for BriqCK, Briq28, and Briq46, respectively. The emission characteristics were distinctly better than those of fluid-bed burners owing to the fact that the heating stove was a static combustion burner without an air-blast system and the fuels were briquetted (Wang et al., 2016).

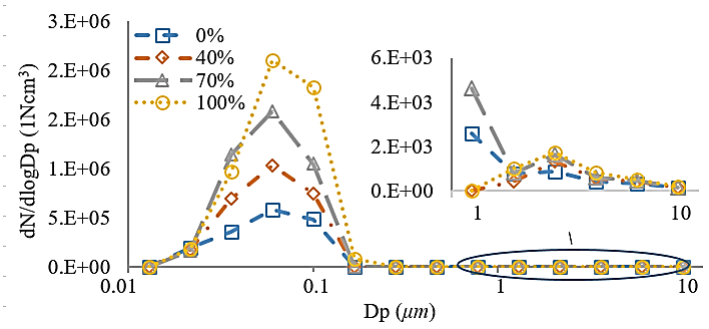

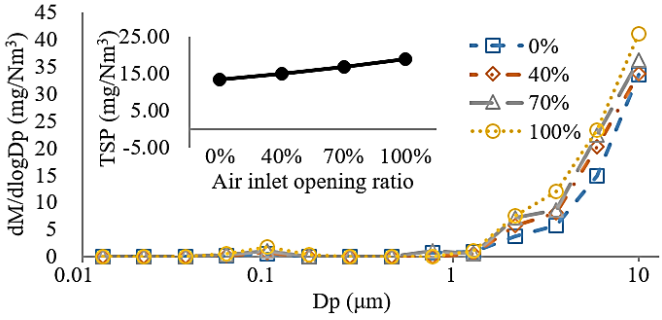

351

352 a. BriqCK

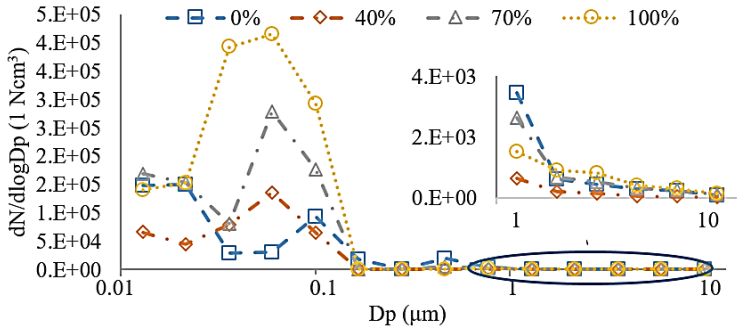

353

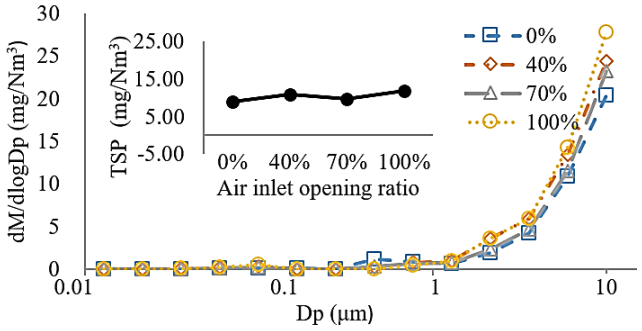

354

355 b. Briq28

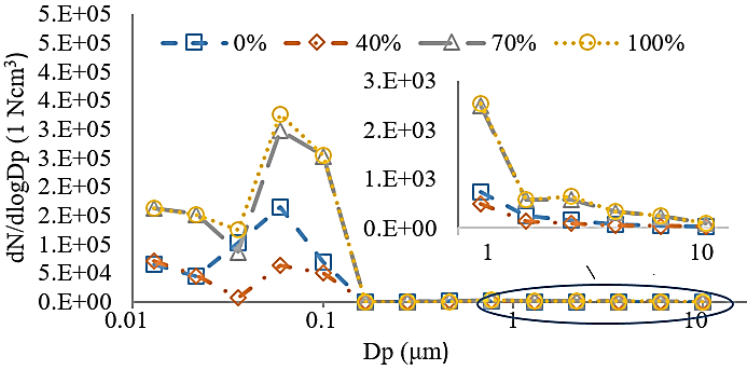

356

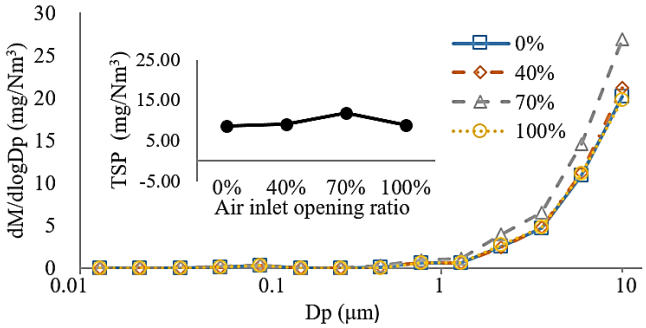

c. Briq46

Fig. 5. Total suspended particles (TSP), number size, and mass size distribution of BriqCK (a), Briq28 (b), and Briq46 (c) under different operation conditions (the air inlet open ratios of 0 %, 40 %, 70 %, and 100 %, respectively).

3.3 Value-chain model design and benefit evaluation

To promote the new heating fuels, which displayed favourable combustion and emission performance, a typical value-chain model that was mainly composed of straw slow pyrolysis, co-densification of char and semi-coke, and utilization of the heating fuels, was designed (Fig. 6). First, crop straws were converted to char, pyrolytic gas, and by-products, e.g., tar and a vinegar-like fraction, using pyrolysis poly-generation technology. Most of the pyrolytic gas was directly burned in a gas burner to produce hot water or hot air for co-densification of the chars and semi-coke, and the surplus was purified and delivered to residents as a clean fuel for cooking or washing. Most of the chars were blended with semi-coke and molded into honeycomb briquettes, which were mainly used for heating via household stoves or boilers. These household stoves were widely used in traditional villages, and the boilers were suitable for new communities with modern facilities and high population densities in

rural China. The remaining fraction of the chars could be used locally as a fertilizer to improve soil structure and fertility. The value-chain model was recyclable, highly efficient, and clean.

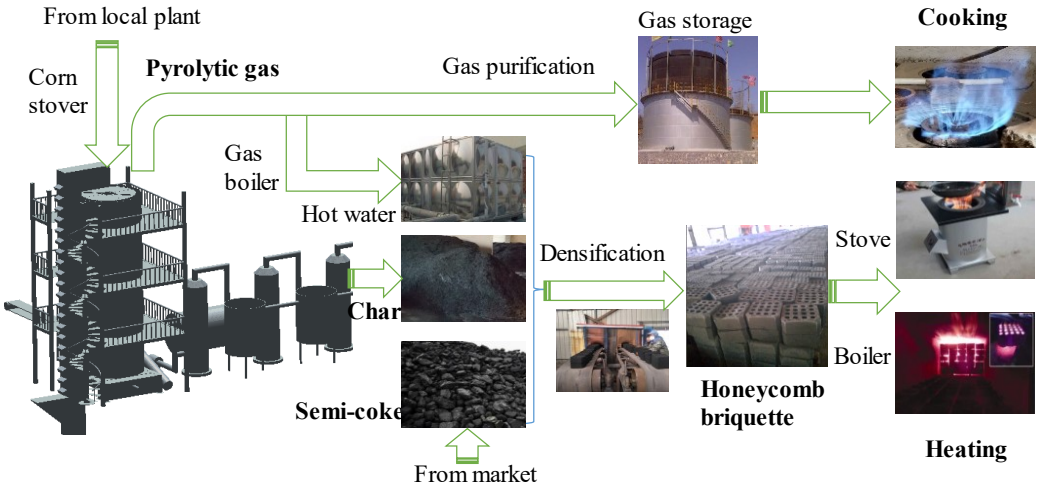

Fig. 6. Value-chain model based on honeycomb briquette and straw slow pyrolysis.

The benefits evaluation in this study was based on a demonstration project using the above value-chain model in Tangshan City, Hebei Province, which went into operation in 2017. This plant was mainly comprised of an internal heating straw pyrolysis production line, pyrolysis gas purification system, honeycomb briquette molding production line, gas burner for hot water or hot air, and two 500 m^3 gas storage tanks. A gas pipeline was laid to a nearby village of about 140 households. The honeycomb briquette molding production line ran for several years before 2017 mainly using semi-coke or anthracite as raw materials.

In order to add approximately 15–20 % straw char to the honeycomb briquettes of

390 semi-coke, the new investment and running costs for producing straw char are shown
391 in Table 4. The new investment costs were approximately $341,000 USD, and the
392 running costs and income per year were $220,200 USD and $67,100 USD,
393 respectively. The utilization amount of crop-straw was about 4,200 t/y; thus,
394 approximately 1,260 t of straw char was produced annually. Most pyrolytic gas was
395 directly burned in a gas burner to produce hot water or hot air, and only about 110,000
396 m^3 of purified gas was piped to residences for cooking. When the equipment
397 depreciation period was 10 y, the production cost of straw char was $134 USD/t, and
398 the cost would decrease to $109 USD/t excluding the equipment depreciation costs.
399 The market prices of semi-coke are about $121–130 USD/t; therefore, if the new
400 investment cost of $341,000 USD or a subsidy of $25 USD/t of straw char were
401 supported by national public finance, then the project would be profitable and run
402 sustainably. The project could increase the income of local farmers by approximately
403 $130,200 USD/y through the sale of crop-straws. Complete utilization of the straw
404 could be achieved, and the rural energy structure and environment would be improved
405 across the project's region. Thus, the social benefits of the project are considerable.
406
407 **Table 4.** Estimation of project investment and running costs for straw char production
408

Items	Details	Income and expenditure	Remarks
New investment (USD)	Straw pyrolysis production line	63,000	The gas pipeline was laid to a nearby village with about 140 households, and the costs of auxiliary equipment (such as
	Gas purification system	12,000	
	Gas boiler for hot water	11,000	

	Gas storage	37,000	stoves) were borne by the residents
	Gas pipeline	210,000	
	Civil engineering	8,000	
Running cost (USD/t)	Materials	130,200	
	Labor	12,000	
	Electricity	63,000	
	Others	15,000	
Income (USD/y)	Fuel gas	5,100	Hot water and hot air were used in the plant, which allowed cost saving compared with the original briquette production system
	Hot water and hot air	62,000	
Production cost of straw char (USD/t)		109	Excluding equipment depreciation costs
		134	Including equipment depreciation costs

Note: The equipment depreciation period is 10 y. The sale price of gas is approximately \$0.05 USD/m^3.

4. Conclusions

The co-combustion characteristics of semi-coke and corn stover char combined in different proportions were tested and analyzed in this study. The results showed that adding 20 % corn stover char (BS28) effectively improved the combustion performance of semi-coke, and this proportion was the ideal mixing ratio. Thus, the integrated combustion characteristics of the blend increased from 5.44×10^{-12} $K^{-3}\cdot min^{-2}$ to 15.08×10^{-12} $K^{-3}\cdot min^{-2}$ for semi-coke.

A honeycomb briquette was developed from a combination of semi-coke and corn stover char for use as a heating fuel in rural China. The emission test results revealed that SO_2 and $PM_{2.5}$ emissions decreased with the addition of corn stover char; however, NO_X emissions increased and the CE decreased slightly with corn stover char addition. The SO_2 concentrations of BriqCK, Briq28, and Briq46 under different experimental conditions were 24.9–26.3, 9.5–16.7, and 5.2–15.4 mg/Nm^3,

respectively, and the NO_X concentrations were 63.1–149.7, 54.3–175.4, and 57.7–168.4 mg/Nm^3, respectively.

A value-chain model for the new heating fuel was developed, and benefits based on a demonstration project in Tangshan City were analyzed. If the new investment cost of $341,000 USD or a subsidy of $25 US/t of straw char were borne by national public finance, then the project would be profitable and run sustainably. This study provided an important technical basis for the development and application of new heating fuels in China.

Acknowledgments

The study benefitted from the technical support provided by the Key Laboratory of Energy Resource Utilization from Agriculture Residue of the Ministry of Agriculture and Rural Affairs, China. The authors would like to thank the laboratory’s staff for their support in the successful completion of this work.

Funding: This work was supported by the China Agriculture Research System [grant number: CARS-02].

References

Barbanera, M., Cotana, F., Di Matteo, U., 2018. Co-combustion performance and kinetic study of solid digestate with gasification biochar. Renew. Energy. 121, 597–605.

Chen, X., 2016. Economic potential of biomass supply from crop residues in China. Appl. Energy. 166, 141–149. https://doi.org/10.1016/j.apenergy.2016.01.034.

Cong, H., Yao, Z., Zhao, L., Jia, J., Lan, S., 2017. Development of carbon, gas and oil polygeneration pilot system based on biomass continuous pyrolysis. Trans. Chin. Soc. Agric. Eng. 33, 173–179.

Courtemanche, B., Levendis, Y., 1998. A laboratory study on the NO, NO_2, SO_2, CO and CO_2 emissions from the combustion of pulverized coal, municipal waste plastics and tires. Fuel. 77, 183–196.

De Soete, G.G., 1991. Heterogeneous N2O and NO formation from bound nitrogen atoms during coal char combustion. Symp. Combust. Proceedings of the 23rd International Symposium on Combustion. The Combustion Institute. https://doi.org/10.1016/S0082-0784(06)80388-7

European Biochar Foundation (EBC), 2018. European Biochar Certificate – Guidelines for a sustainable production of biochar. http://www.european-biochar.org/en/download (accessed 30 August 2018).

Gómez, N., Rosas, J.G., Cara, J., Martínez, O., Alburquerque, J.A., Sánchez, M.E., 2016. Slow pyrolysis of relevant biomasses in the Mediterranean Basin. Part 1. Effect of temperature on process performance on a pilot scale. J. Clean. Prod. 120, 181–190.

Hu, Q., Shao, J., Yang, H., Yao, D., Wang, X., Chen, H., 2015. Effects of binders on the properties of bio-char pellets. Appl. Energy. 157, 508–516. https://doi.org/10.1016/j.apenergy.2015.05.019.

Jie, T., Haiyan, N., Yongming, H., Zhenxing, S., Qiyuan, W., Xin, L., 2018. Primary $PM_{2.5}$ and trace gas emissions from residential coal combustion: Assessing semi-coke briquette for emission reduction in the Beijing-Tianjin-Hebei region, China. Atmos. Environ. 191, 378–386.

Jin, Y., Li, Y., Liu, F., 2016. Combustion effects and emission characteristics of SO_2, CO, NO_X and heavy metals during co-combustion of coal and dewatered sludge. Front. Environ. Sci. Eng. 10, 201–210.

Klinghoffer, N., Castaldi, M.J., Nzihou, A., 2011. Beneficial Use of ash and char from biomass gasification. 14 Proceedings of the 19th Annual North American Waste-to-Energy Conference. https://doi.org/10.1115/nawtec19-5421

Kua, H.W., Pedapati, C., Lee, R.V., Kawi, S., 2019. Effect of indoor contamination on carbon dioxide adsorption of wood-based biochar – Lessons for direct air capture. J. Clean. Prod. 210, 860–871.

Li, H.J., Zhi, S.W., Li, L.J., Lu, H.E., Yue, M.A., Yuan, L.S., 2016. Comparison of emission from lantan (semi-coke) instead of raw coal for clean and efficient combustion. Coal Technol. 35, 287–289. https://doi:1 .13301/j.cnki.ct.2016.08.118.

Li, L., Zou, D., Xiao, Z., Zeng, X., Zhang, L., Jiang, L., Wang, A., Ge, D., Zhang, G., Liu, F., 2019. Biochar as a sorbent for emerging contaminants enables improvements in waste management and sustainable resource use. J. Clean. Prod. 210, 1324–1342. https://doi.org/10.1016/j.jclepro.2018.11.087.

Li, Q., Li, X., Jiang, J., Duan, L., Ge, S., Zhang, Q., Deng, J., Wang, S., Hao, J., 2016. Semi-coke briquettes: Towards reducing emissions of primary $PM_{2.5}$, particulate carbon, and carbon monoxide from household coal combustion in China. Sci. Rep. 1, 19306 https://doi.org/10.1038/srep19306.

Liu, X., Chen, M.Q., Wei, Y.H., 2015. Kinetics based on two-stage scheme for co-combustion of herbaceous biomass and bituminous coal. Fuel. 143, 577–585.

Ministry of Agriculture of the People's Republic of China (MOA), 2016. China's main crop straw comprehensive utilization rate exceeds 80 % (in Chinese). http://jiuban.moa.gov.cn/zwllm/zwdt/201605/t20160526_5151375.htm (accessed 26 May 2016).

Ministry of Environmental Protection of the People's Republic of China (MEP), 2016. Pollution comprehensive management for residential coal combustion (in Chinese). http://www.mep.gov.cn/gkml/hbb/bgg/201610/t20161031_366528.htm (accessed 21 May 2016).

Moon, C., Sung, Y., Ahn, S., Kim, T., Choi, G., Kim, D., 2013. Effect of blending ratio on combustion performance in blends of biomass and coals of different ranks. Exp. Therm. Fluid Sci. 47, 232–240.

Mourant, D., Wang, Z., He, M., Wang, X.S., Garcia-Perez, M., Ling, K., Li, C.Z., 2011. Mallee wood fast pyrolysis: Effects of alkali and alkaline earth metallic species on the yield and composition of bio-oil. Fuel. 90, 2915–2922.

National Energy Administration (NEA), 2016. Notice on printing and distributing the 13th Five-Year Plan for Energy Development (in Chinese). http://www.ndrc.gov.cn/zcfb/zcfbtz/201701/t20170117_835278.html (accessed 26 December 2016).

National Energy Administration (NEA), 2017. Notice on printing and distributing guidance on promoting biomass energy heating development (in Chinese). http://zfxxgk.nea.gov.cn/auto87/201712/t20171228_3085.htm (accessed 06 December 2017).

512 Niu, S., Chen, M., Li, Y., Song, J., 2017. Co-combustion characteristics of municipal sewage
513 sludge and bituminous coal. J. Therm. Anal. Calorim. 1, 1–14.

514 Peng, X.W., Ma, X.Q., Xu, Z.B., 2015. Thermogravimetric analysis of co-combustion
515 between microalgae and textile dyeing sludge. Bioresour. Technol. 180, 288–295.

516 Phusrimuang, J., Wongwuttanasatian, T., 2016. Improvements on thermal efficiency of a
517 biomass stove for a steaming process in Thailand. Appl. Therm. Eng. 98, 196–202.

518 Ren, X., Sun, R., Meng, X., Vorobiev, N., Schiemann, M., Levendis, Y.A., 2017. Carbon,
519 sulfur and nitrogen oxide emissions from combustion of pulverized raw and torrefied
520 biomass. Fuel. 188, 310–323. https://doi.org/10.1016/j.fuel.2016.10.017.

521 Roy, M.M., Corscadden, K.W., 2012. An experimental study of combustion and emissions of
522 biomass briquettes in a domestic wood stove. Appl. Energy. 99, 206–212.
523 https://doi.org/10.1016/j.apenergy.2012.05.003.

524 Sarkar, P., Sahu, S.G., Mukherjee, A., Kumar, M., Adak, A.K., Chakraborty, N., Biswas, S.,
525 2014. Co-combustion studies for potential application of sawdust or its low temperature char
526 as co-fuel with coal. Appl. Therm. Eng. 63, 616–623.

527 Schmidt, G., Trouvé, G., Leyssens, G., Schönnenbeck, C., Genevray, P., Cazier, F., Dewaele,
528 D., Vandenbilcke, C., Faivre, E., Denance, Y., Le Dreff-Lorimier, C., 2018. Wood washing:
529 Influence on gaseous and particulate emissions during wood combustion in a domestic pellet
530 stove. Fuel Process. Technol. 120, 15–27. https://doi.org/10.1016/j.fuproc.2018.02.020.

531 Sun, J., Peng, H., Chen, J., Wang, X., Wei, M., Li, W., Yang, L., Zhang, Q., Wang, W.,
532 Mellouki, A., 2016. An estimation of CO_2 emission via agricultural crop residue open field
533 burning in China from 1996 to 2013. J. Clean. Prod. 112, 2625–2631.
534 https://doi.org/10.1016/j.jclepro.2015.09.112.

535 Tarelho, L.A.C., Matos, M.A.A., Pereira, F.J.M.A., 2005. The influence of operational
536 parameters on SO_2 removal by limestone during fluidized bed coal combustion. Fuel Process.
537 Technol. 86, 1385–1401.

538 The State Council the People's Republic of China (SCP), 2017. Notice on printing winter
539 heating plan for the northern region (2017–2021) (in Chinese).
540 http://www.gov.cn/xinwen/2017-12/20/content_5248855.htm (accessed 20 December 2017).

541 Toscano, G., Duca, D., Amato, A., Pizzi, A., 2014. Emission from realistic utilization of
542 wood pellet stove. Energy. 68, 466–650. https://doi.org/10.1016/j.energy.2014.01.108.

543 Wang, J., Lou, H.H., Yang, F., Cheng, F., 2016. Development and performance evaluation of
544 a clean-burning stove. J. Clean. Prod. 134(Part B), 447–455.

Wang, W., Wena, C., Li, C., Wang, M., Li, X., Zhou, Y., Gong, X., 2019. Emission reduction of particulate matter from the combustion of biochar via thermal pre-treatment of torrefaction, slow pyrolysis or hydrothermal carbonization and its co-combustion with pulverized coal. Fuel. 240, 278–288.

Werther, J., Saenger, M., Hartge, E.U., Ogada, T., Siagi, Z., 2000. Combustion of agricultural residues. Prog. Energy Combust. Sci. 26, 1–27.

Xing, X., Cheng, Z., Li, Y., Zhu, C., Zhang, X., 2019. Co-combustion characteristics and kinetic analyses of rice straw and pulverized coal. Chin. J. Process Eng. 19, 637–643. https://doi.org/10.12034/j.issn.1009-606X.218277.

Yank, A., Ngadi, M., Kok, R., 2016. Physical properties of rice husk and bran briquettes under low pressure densification for rural applications. Biomass Bioenergy. 64, 22–30. https://doi.org/10.1016/j.biombioe.2015.09.015.

Zhang, S., Jiang, X., Lv, G., 2019. Co-combustion of Shenmu coal and pickling sludge in a pilot scale drop-tube furnace: Pollutants emissions in flue gas and fly ash. Fuel Process. Technol. 184, 57–64.

Zhang, S., Jiang, X., Lv, G., Liu, B., Jin, Y., Yan, J., 2016. SO_2, NO_X, HF, HCl and PCDD/Fs emissions during co-combustion of bituminous coal and pickling sludge in a drop tube furnace. Fuel. 186, 91–99.

Zhao, P., Shen, Y., Ge, S., Chen, Z., Yoshikawa, K., 2014. Clean solid biofuel production from high moisture content waste biomass employing hydrothermal treatment. Appl. Energy. 131, 345–367.

Zheng, D., Lu, H., Sun, X., Liu, X., Han, W., Wang, L., 2013. Reaction mechanism of reductive decomposition of FGD gypsum with anthracite. Thermochim. Acta. 559, 23–31.

Declarations of interest: none.